Preprint Cambridge Centre for Computational Chemical Engineering ISSN 1473 – 4273

Modelling Soot Formation: Model of Particle Formation

Edward K. Y. Yapp, Markus Kraft [1]

released: 7 October 2013

[1] Department of Chemical Engineering
and Biotechnology
University of Cambridge
New Museums Site
Pembroke Street
Cambridge, CB2 3RA
United Kingdom
E-mail: mk306@cam.ac.uk

Preprint No. 134

Edited by
Computational Modelling Group
Department of Chemical Engineering and Biotechnology
University of Cambridge
New Museums Site
Pembroke Street
Cambridge CB2 3RA
United Kingdom

Fax: + 44 (0)1223 334796
E-Mail: c4e@cam.ac.uk
World Wide Web: http://como.cheng.cam.ac.uk/

Abstract

This article reports on detailed models of soot particle formation in combustion. First, we present the polycyclic aromatic hydrocarbon-primary particle (PAH-PP) model where soot particles are described by primary particles which are made up of PAHs. The model describes the formation, growth and oxidation of soot in laminar premixed ethylene flames. The connectivity between primary particles is stored to calculate the rounding of soot particles due to surface growth and condensation. We then show that a model intermolecular potential based on the simple Lennard-Jones potential supports the physical binding of PAHs as a viable mechanism for soot formation. We subsequently present the kinetic Monte Carlo-aromatic site (KMC-ARS) model which describes the structure and growth of planar PAHs. The PAH processes are represented as jump processes, and the energetics and kinetics were determined by quantum chemistry calculations. Lastly, we use molecular dynamics with a new potential specifically developed for PAH interaction and the combined PAH-PP/KMC-ARS model to show that pyrene dimerisation is unlikely to be the critical soot formation step at flame temperatures of about 1500–2000 K.

Contents

1 Introduction **3**

2 Model of the Formation, Growth and Oxidation of Soot Particles in Laminar Premixed Ethylene Flames **3**

3 Model Intermolecular Potential Describing the Physical Binding of PAHs **7**

4 Model of the Gas-Phase Interactions of PAHs **9**

5 Critical Soot Formation Size **12**

5.1 Polycyclic Aromatic Hydrocarbon Anisotropic Potential 12

5.2 Combined PAH-PP/KMC-ARS Model 14

6 Conclusion **16**

7 Final remarks **16**

References **19**

1 Introduction

This article presents some recent results relevant to the modelling of the formation of soot particles in flames.

A detailed population balance model is introduced to bridge the gap between particle population dynamics and gas-phase reactions. A basin-hopping optimisation technique is used to provide insight into the structure of nascent soot particles. Quantum chemistry and kinetic Monte-Carlo (KMC) simulations are employed to describe growth and oxidation rates of polycyclic aromatic hydrocarbons (PAHs) in flames. Finally, using all model components described above, the critical size of PAHs which can form a soot particle is investigated (a) by using molecular dynamics (MD) simulations and (b) by fitting the detailed population balance model to mass spectrometry data.

2 Model of the Formation, Growth and Oxidation of Soot Particles in Laminar Premixed Ethylene Flames[1]

In this section, the formation, growth and oxidation of soot in a laminar premixed flame is described in terms of a detailed population balance model named polycyclic aromatic hydrocarbon-primary particle (PAH-PP) and the laminar flame solver PREMIX.

The PAH-PP model is a detailed soot particle model where soot particles are represented by primary particles made up of PAHs. As each individual PAH in a soot particle is tracked, a detailed chemical model describing the interactions of the soot particle with the gas-phase can be incorporated. The chemical model used here is the kinetic Monte-Carlo-aromatic site (KMC-ARS) model, which is described in Sect. 4. It is assumed that the first soot particles are formed from gas-phase species. In the case of a premixed laminar flame, the concentration of pyrene ($C_{16}H_{10}$) is precalculated using PREMIX [11] and read in as an input to the model. PREMIX is a one-dimensional laminar flame solver, which solves for the gas-phase chemical species and the first six moments of the soot particle size distribution (PSD) based on a spherical particle model [1]. Further growth of these molecules is calculated using the KMC-ARS model. This growth happens either in the gas phase or, if the PAH is part of a soot particle, in the particle itself.

Figure 1 shows the different transformation processes in the model. These processes are summarised below:

Formation. A soot particle forms when two PAH molecules stick after collision. In the model, a size and mass-dependent collision efficiency determines the probability of sticking (see Sect. 5.2). The sticking of two PAHs incepts a soot particle consisting of one primary particle which is made up of the two PAHs.

Coagulation. Two particles P_i and P_j collide creating a new particle P_k. It is assumed that one primary particle p_a of P_i and one primary particle p_b of P_j are in point contact in the new particle P_k.

[1] All material has been drawn from Sander [20] unless otherwise indicated.

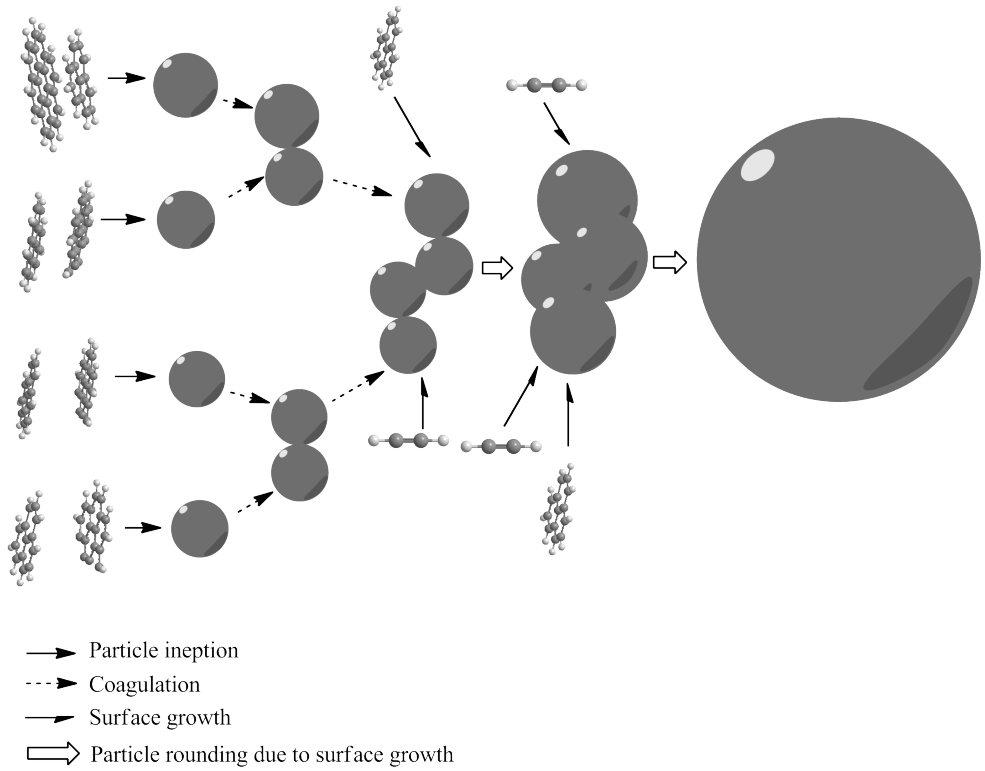

Figure 1: *Transformation processes in the PAH-PP model (Sander et al. [21]; Copyright Elsevier)*

Condensation. PAHs from the gas-phase condense onto the particles increasing the mass and sphericity (rounding) of the particle. It is implemented in the model by adding the gas-phase PAH to primary particle p_a within particle P_i.

Surface growth. PAHs in the soot particle react with the gas-phase. However, possibly due to steric hindrance, PAHs within the soot particle do not grow as quickly as PAHs in the gas-phase. To account for this the growth rate of PAHs within soot particles is multiplied by a growth factor g.

Soot particles increase in sphericity due to surface growth and condensation. Because the connectivity between primary particles is stored using a binary tree structure, the neighbours of each particle is known and a rounding factor r can be applied to any two neighbouring primary particles.

The particle population dynamics and the evolution of PAHs were recently coupled in the work by Chen et al. [3]. In the previous implementation, PAH growth is precalculated using the KMC-ARS model and the evolution of PAHs is stored in databases for various heights along the flame. The particle population dynamics is approximated by moving a sample volume containing stochastic particles through the flame at a gas velocity specified in PREMIX. Every pyrene molecule "transferred" into the particle model is assigned an evolution history from the database. In the current implementation, the evolution of PAHs is calculated during the simulation. A further process to be added is fragmentation where large aggregates break down into smaller aggregates which can be important in premixed

flames [14].

The population balance describing the inception, coagulation, condensation and surface growth processes is solved using the direct simulation Monte-Carlo (DSMC) method; also called the direct simulation algorithm (DSA). The numerical solution of the population balance when using the PAH-PP model includes the following steps:

(1) Set start time $t \leftarrow t_0$ and initial position along the flame $x \leftarrow x_0$.

(2) Calculate the rates R_i of formation, condensation and coagulation (described below).

(3) Calculate an exponentially distributed waiting time dt with parameter:

$$R_{\text{tot}} = \sum R_i, \tag{1}$$

where R_i are the rates of the individual processes.

(4) Increase time by the waiting time $t \leftarrow t + \mathrm{d}t$ and update the position x.

(5) Update the evolution of all the PAHs in the particles or in the gas-phase through the KMC-ARS model.

(6) If $t \geq t_{\text{stop}}$ then end.

(7) A process i is selected based on the probability:

$$P = \frac{R_i}{R_{\text{tot}}}. \tag{2}$$

(8) Perform the process.

(9) Go to step 2.

The rates of formation, condensation and coagulation are calculated from the transition-regime kernel K^{tr} and are premultiplied by a sticking efficiency. K^{tr} is calculated as the harmonic mean of kernels K^{sf} and K^{fm}:

$$K^{\text{tr}}(A,B) = \frac{K^{\text{sf}}(A,B)K^{\text{fm}}(A,B)}{K^{\text{sf}}(A,B) + K^{\text{fm}}(A,B)}. \tag{3}$$

For a formation process, A and B represent PAHs; for a condensation process, A is a particle and B is a PAH, or vice versa; for a coagulation process, A and B are particles. The slip-free kernel K^{sf} and the free-molecular kernel K^{fm} are calculated as follows:

$$K^{\text{sf}}(A,B) = \frac{2k_{\text{B}}T}{3\mu}\left(\frac{1+1.257Kn_A}{d_{\text{c}}(A)} + \frac{1+1.257Kn_B}{d_{\text{c}}(B)}\right)(d_{\text{c}}(A) + d_{\text{c}}(B)), \tag{4}$$

$$K^{\mathrm{fm}}(A,B) = 2.2\sqrt{\frac{\pi k_{\mathrm{B}} T}{2}}\left(\frac{1}{M(A)}+\frac{1}{M(B)}\right)^{\frac{1}{2}}(d_{\mathrm{c}}(A)+d_{\mathrm{c}}(B))^2, \tag{5}$$

where k_{B} is the Boltzmann constant; T is temperature; μ is the dynamic viscosity of the gas-phase; Kn_x is the Knudsen number of a PAH or particle x; and $M(x)$ and $d_{\mathrm{c}}(x)$ is the mass and collision diameter, respectively, of a particle or PAH, x. The Knudsen number can be easily calculated from the diameter of the particle. Correlations for the collision diameters have been determined by Sander et al. [21].

Figure 2 shows an example of a soot particle generated using the PAH-PP model. The connectivity between primary particles is clearly shown and a count of a selection of PAHs (sorted by the number of carbon (C) atoms it contains) for two particular primary particles is shown as well.

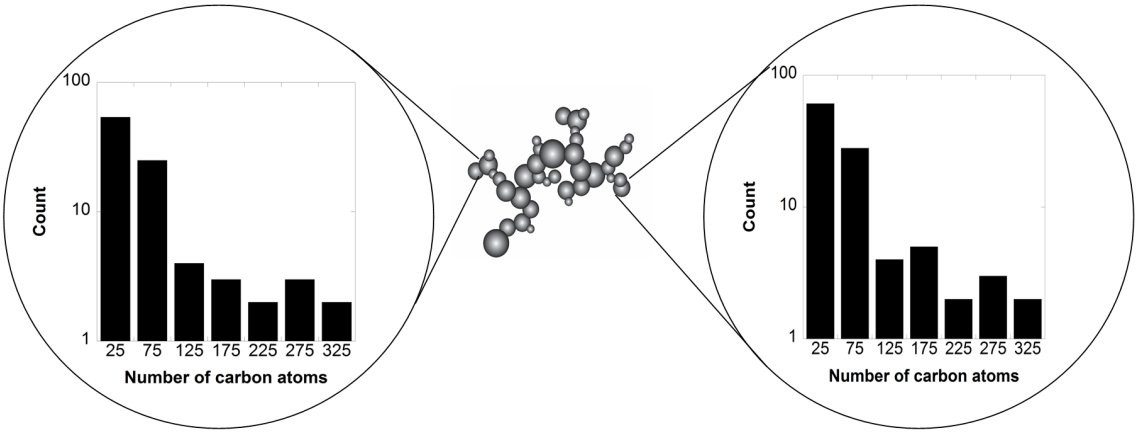

Figure 2: *A soot particle generated using the PAH-PP model and the detailed information stored for each primary particle (Sander et al. [21]; Copyright Elsevier)*

Three parameters in the PAH-PP model [21]: soot density ρ, growth factor g and rounding factor r were determined empirically by fitting the median of the logarithmic part of the PSD to a number of laminar premixed ethylene flames [29]. A low discrepancy series method was applied followed by a quadratic response surface optimisation. The shape of the PSD of large particles was well-matched but the number density of smaller particles was underpredicted. The results of the fitting procedure suggest that almost all the chemical growth takes place in the gas-phase and not inside the particle. Further, it indicates that the value of the soot density is around 1.5 g/cm^3, which is slightly below the commonly assumed value of 1.8 g/cm^3.

3 Model Intermolecular Potential Describing the Physical Binding of PAHs[2]

The purpose of this section is to find possible PAH configurations which minimise their potential energy surface and investigate the density of such a PAH structure.

The PAH-PP model describes the population dynamics of soot particles, i.e. their formation, growth, shape evolution and oxidation. However, the mechanism of how PAHs stick together is not quite understood and there is a need to refine the sub-models for particle formation and the models for which intra- and interparticle molecular mobility plays a role. The forces that drive the interactions of molecules are determined by intermolecular potentials.

Intermolecular interactions describe the sum of attractive and repulsive forces between molecules. For large systems of molecules, the only computationally feasible approach to describe these interactions is to use model potentials. The total interaction energy of a molecular cluster can be approximated as the sum over all pairwise atom-atom interactions between atom a of molecule A and atom b of molecule B:

$$U = \sum_{A} \sum_{A<B} \sum_{a \in A} \sum_{b \in B} U_{ab}(R_{ab}, \Omega_{ab}), \tag{6}$$

where $U_{ab}(R_{ab}, \Omega_{ab})$ is the atom-atom interaction potential as some function of the atom-atom separation R_{ab} and their relative molecular orientation Ω_{ab}. Each molecule is treated as a rigid body, thereby ignoring intramolecular degrees of freedom.

A popular form for U_{ab} is the isotropic Lennard-Jones (LJ) potential plus point charge electrostatic model:

$$U_{ab} = U_{\mathrm{LJ}} + U_{\mathrm{elec}} = 4\varepsilon_{ab} \left[\left(\frac{\sigma_{ab}}{R_{ab}} \right)^{12} - \left(\frac{\sigma_{ab}}{R_{ab}} \right)^{6} \right] + \frac{q_a q_b}{R_{ab}}, \tag{7}$$

where ε_{ab} and σ_{ab} are the potential well-depth and size parameters, respectively, describing interactions between atoms a and b. These parameters have been empirically determined for hydrocarbons [26]: CC, CH and HH atom-atom interactions. The R^{-12} term represents repulsion while the R^{-6} term represents dispersion. q_a and q_b are partial charges on atoms a and b.

To calculate the optimal arrangement of several PAH molecules the LJ potential plus point-charge electrostatic model is used to generate a potential energy surface (PES) for a molecular cluster of PAHs. The PES is then transformed into a discrete set of energy levels by applying a global optimisation technique using a "basin-hopping" scheme [27]. The technique involves perturbing the geometry of the cluster and carrying out a minimisation on the resulting geometry. A step is accepted if the energy of the new geometry is less than at the previous step. If the energy of the new geometry is greater than before, an accept-reject scheme such as the Metropolis criterion is used [12] which helps the basin-hopping

[2] All material has been drawn from Totton et al. [24] unless otherwise indicated.

scheme to move through successive local minima.

Figure 3 shows the low energy cluster arrangement of pyrene and coronene. These two types of soot precursors are typically found in flame environments. Clusters of only 50 PAHs were considered because simulating larger systems would be computationally expensive. In reality, soot particles contain hundreds, if not, thousands of PAHs. In the simulations, the PAHs were initially randomly scattered whilst ensuring no molecular overlap. Note the formation of multiple stacks (PAHs aligned parallel to each other) made up of 2–4 PAHs. This approach was used to study homomolecular clusters but can be easily extended to the study of mixtures of PAHs.

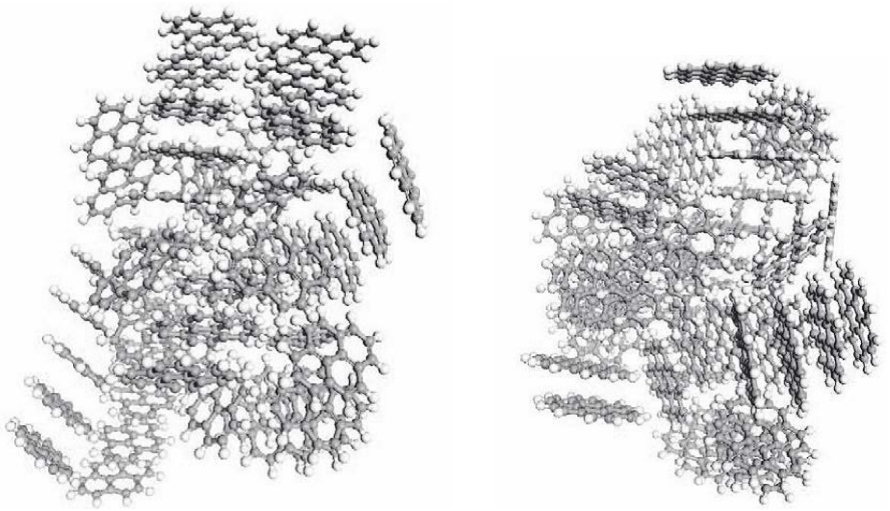

(a) **(b)**

Figure 3: *Low energy cluster arrangement of* **a** *50 pyrene molecules ($C_{16}H_{10}$) and* **b** *coronene ($C_{24}H_{12}$) molecules, found using model intermolecular potential (Totton et al. [24]; Copyright Elsevier)*

Figure 4 shows a computationally generated transmission electron microscope (TEM) image of 50 coronene molecules compared against two experimental HR-TEM images of soot aggregates sampled from a diesel engine [13]. While the experimental images suggest the presence of larger PAH structures, on the length scale of 2.5–3.0 nm, they show the formation of stacks and there is a qualitative agreement in the number of PAHs in each stack and the separation between the molecular planes.

These images clearly show the sticking of PAHs inside a soot particle and there is strong support for the physical binding of two PAHs as a viable mechanism for soot formation. Soot density is an important parameter in the PAH-PP model and a value of around 1.8 g/cm^3 is commonly used. By defining a critical scaling factor such that all intermolecular space within a cluster is occupied, an improved estimate of soot density can be calculated. The density of a 50 coronene cluster, taken to be representative of a nascent soot particle, was calculated to be 1.12 g/cm^3.

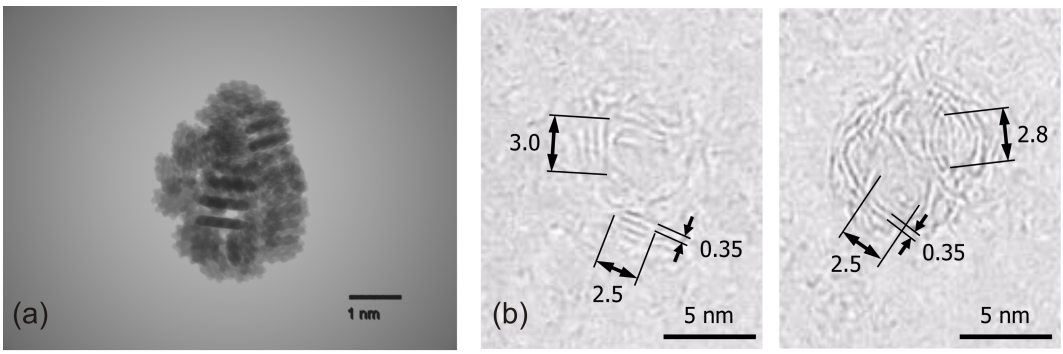

Figure 4: **a** *TEM-style projection of a cluster of 50 coronene molecules using model intermolecular potential (Totton et al. [24]; Copyright Elsevier) and* **b** *experimental TEM images of soot aggregates sampled from a diesel engine (Mosbach et al. [13]; Copyright Elsevier)*

4 Model of the Gas-Phase Interactions of PAHs[3]

The chemical growth of PAHs is represented by the KMC-ARS model. The KMC-ARS model describes the structure and growth of planar PAH structures [16]. A PAH is assumed to be fully represented by the number of C and hydrogen (H) atoms it contains, and the number and types of elementary sites on its edge. Figure 5 shows the four elementary sites [2]: free-edge, zig-zag, armchair and bay sites. A five-member ring is to be distinguished from the other sites because it may occupy a zig-zag site [6]. Each site has exactly two surface C atoms (bonded to a H atom) and is distinguished by the number of bulk C atoms (not bonded to a H atom). For example, a free-edge site has zero bulk C atoms, while a zig-zag site has one bulk atom; both sites have two surface C atoms.

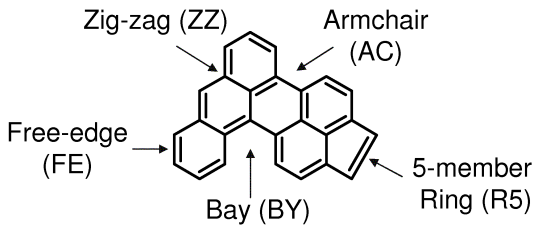

Figure 5: *PAH showing the different types of elementary sites on which different reactions and jump processes can take place in the KMC-ARS model (Raj et al. [16]; Copyright Elsevier)*

This model simulates the growth of a PAH through a detailed set of PAH surface reactions and jump processes which are solved using the KMC algorithm. The surface reactions are assumed to take the modified Arrhenius form and the rate constant of each reaction is calculated as:

$$k(T) = AT^n \exp\left(\frac{-E}{RT}\right), \tag{8}$$

[3] All material has been drawn from Raj et al. [16] unless otherwise indicated.

where A is the temperature-independent constant, T is the temperature, n is a constant, E is the activation energy and R is the universal gas constant.

A PAH may undergo different processes such as five-member and six-member ring addition, removal and oxidation at different reactive sites. Each of these processes is made up of a number of reversible and/or irreversible surface reactions. Including all the intermediate species in the reaction mechanism would be computationally unfeasible. Therefore, the intermediate species are assumed to be at steady-state, and ring addition and removal steps are assumed to be irreversible; hence, the name *jump* process. The jump processes are defined such that they take place only on certain sites or parent sites. A parent site is defined as a site on which a reaction takes place and is replaced in the reaction. The rate of a jump process at a parent site is calculated as:

$$R_i = k_i \times f_i \times C \times N_{\text{site}}(e), \tag{9}$$

where k_i is the rate constant from Eq. 8 and f_i is the fraction of radical sites of the parent type found using the steady-state assumption [2]. f_i is calculated as some function of the concentrations of the intermediate species and rate constants; C is the concentration of the gas-phase species involved in the reaction. $N_{\text{site}}(e)$ is the number of parent sites on the PAH as some function of the data structure e, which will be explained below.

The KMC algorithm allows the structure of a PAH to be tracked explicitly but is limited to single planar PAHs. The model is formulated mathematically by first defining a data structure, then defining the jump processes and each corresponding rate on the basis of this structure. However to derive a suitable data structure, the concept of a state space is first introduced.

The state space refers to all possible states in the system and each state corresponds to a unique point. The simplest state space is made up of the following state variables: positions of the C atoms and the bonds between them. Each C atom is assumed to be sp^2 hybridised which means that each bulk C atom is bonded to three other C atoms; while a C atom on the surface of the PAH is bonded to two other C atoms (and a H atom depending on whether a radical site is created.) The state space for a 2D representation of planar or near-planar PAHs can be represented as [7]:

$$E = (i, j, i_1, j_1, i_2, j_2, i_3, j_3), \tag{10}$$

where i and j are the x and y coordinates, respectively, of a C atom, and i_n and j_n are the coordinates of the nth C atom bonded to the C atom with coordinates (i, j). Note that information about the bonds between C atoms is implied by the relative positions of the C atoms. For a surface C atom coordinates (i_3, j_3) are set to some pre-defined value.

For PAHs with a 3D geometry, such as a five-membered ring surrounded by five six-membered rings, additional coordinates can be added to the state space. However, the KMC algorithm may not be applicable and MD may be required to determine the resulting structure [18]. This state space provides sufficient information for the jump processes to be defined but it is difficult to do so; therefore, a higher-order data structure is required.

A 2D grid is generated and a single PAH is placed on this grid. Each C atom in the PAH

is assigned a grid point and its structure is fully described by the data structure:

$$e = (c, s). \tag{11}$$

It is made up of a C atom vector:

$$c = (S_1, S_2, S_{\text{in}_1}, S_{\text{in}_2}, C_{\text{type}}, i, j), \tag{12}$$

where each surface C atom is part of two elementary sites S_1 and S_2, and S_{in_1} and S_{in_2} are the indices of each site. C_{type} is used to differentiate between a surface and a bulk C atom, and (i,j) are its coordinates.

And a site vector:

$$s = (S_{\text{type}}, S_{\text{in}}, i_1, j_1, i_2, j_2), \tag{13}$$

where S_{type} and S_{in} have been defined above, and each site has two surface C atoms which have coordinates (i_1,j_1) and (i_2,j_2).

The KMC algorithm is similar to the algorithm used in the PAH-PP model (Sect. 2) but the key differences are: (1) instead of initialising at some position along the flame in the PAH-PP model, a planar PAH is used to initialise e; (2) the rate of each jump process is calculated and based on a probability calculated using this rate a process is selected; (3) vector c is updated when a jump process results in C addition or removal; and (4) vector s is updated when a parent site is replaced and neighbouring sites change.

In the development of a reaction mechanism both the energetics and kinetics of the reactions are required. Quantum chemistry calculations, employing density functional theory (DFT), are performed to predict the geometry and energy of stable molecular species. The potential energy surfaces from these calculations are used to evaluate the rate constants of the surface reactions that take place on a PAH using transition state theory (TST).

Figure 6 is a potential energy diagram constructed from the energies of the reactants, transition states and products. It shows the oxidation of a five-membered ring in chemical species 9 (CS9) by O_2 to form 4-phenanthryl (CS14). This is part of one of the suggested pathways for the assumed model reaction for soot oxidation [19]:

$$\text{4-pyrenyl} + O_2 \rightarrow \text{4-phenanthryl} + 2\text{CO}.$$

In their work, molecular structures were optimised using the B3LYP functional and the 6-311++G(d,p) basis set. The stable chemical species were optimised with different spin multiplicities to determine the multiplicity with the minimum energy and reasonable geometry. The same approach was used in the development of additional dehydrogenation jump processes to improve model predictions [17]. Future work involves constructing jump processes from oxidation reactions, such as the one above, and incorporating them into the KMC-ARS model.

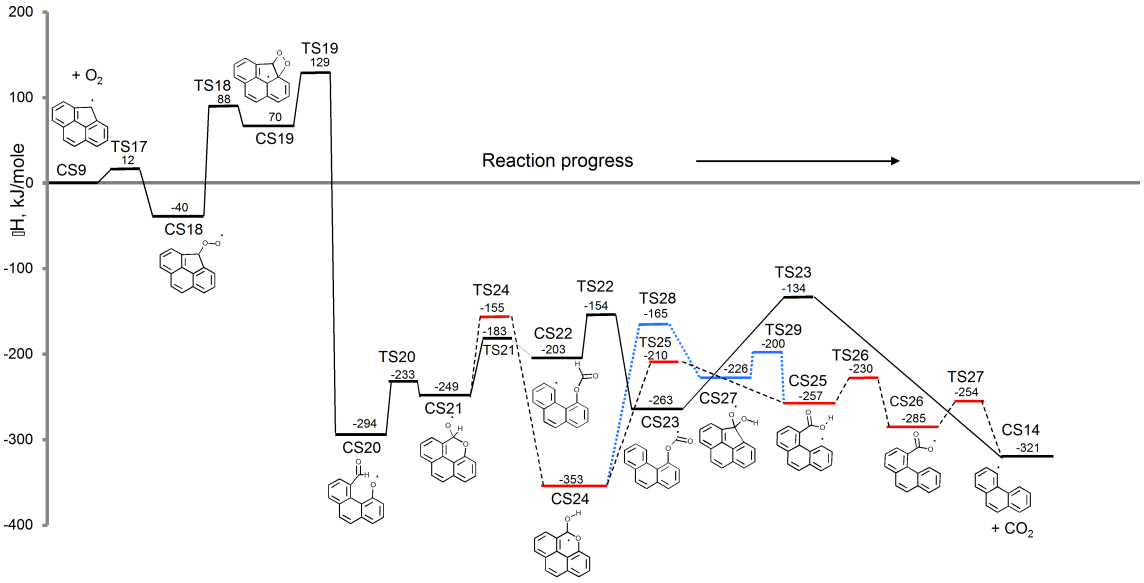

Figure 6: *Potential energy diagram of a suggested pathway for soot oxidation (Raj et al. [16]; Copyright Elsevier)*

5 Critical Soot Formation Size

It is often assumed that pyrene dimerisation is the critical soot particle formation step. However, more recently, there are a number of studies which challenge this view. In the next two sections we lay out two approaches which show that pyrene dimerisation may not be the critical step in the formation of soot at flame temperatures.

5.1 Polycyclic Aromatic Hydrocarbon Anisotropic Potential[4]

The computationally efficient and popular LJ potential may have been acceptable in Sect. 3, but a more accurate potential which considers the intermolecular forces between PAHs is required for the study of the critical soot formation size.

The LJ potential has a tendency to overestimate the well depths of interactions or binding energy between PAH molecules. This would lead to an underestimation of the critical soot formation size at typical flame temperatures of approximately 1500–2000 K [28]. A highly accurate quantum chemistry technique such as symmetry adapted perturbation theory (SAPT(DFT)) would have been ideal but is not feasible for large systems. The next best alternative is a simple potential parameterised using high-accuracy interaction energies of smaller PAHs calculated using SAPT(DFT). Totton et al. [25] used this method to develop the general PAHAP potential which is based on the same three types of interactions (CC, CH and HH atom-atom pairs) as the LJ potential:

$$U_{ab} = G\exp[-\alpha_{ab}(R_{ab} - \rho_{ab}(\Omega_{ab}))] - f_6(R_{ab})\frac{C_{6,\mathrm{iso}}}{R_{ab}^6} + \frac{q_a q_b}{R_{ab}}. \tag{14}$$

[4] All material has been drawn from Totton et al. [25] unless otherwise indicated.

The first term on the right-hand side is the short-range exchange-repulsion term and is modelled using an anisotropic Born-Mayer term. G is a constant energy unit and is set to 0.001 Ha. α_{ab} describes the hardness of the interaction between atoms a and b. The second term is the long-range dispersion term and is modelled using the isotropic coefficient $C_{6,\mathrm{iso}}$ and the damping function $f_6(R_{ab})$ proposed by Tang and Toennies [23]. The third term is the point-charge electrostatic model as in Eq. 7.

The PAHAP potential describes atomic shape anisotropy using angular expansions, but this feature is not currently supported by standard MD codes. Hence, an isotropic PAHAP potential is developed by neglecting the orientation dependence of the shape function ρ_{ab}. The isotropic potential parameters are fitted by calculating the interaction energies for coronene dimers in a variety of conformations. The resulting parameterisation is shown to accurately account for the interactions of other PAHs. Therefore, the isotropic PAHAP potential is transferable to PAHs other than coronene.

The thermodynamics of the homomolecular dimerisation of five representative PAHs was studied across a temperature range of 0–2500 K. Pyrene ($C_{16}H_{10}$), coronene ($C_{24}H_{12}$), ovalene ($C_{32}H_{14}$), hexabenzocoronene ($C_{42}H_{18}$) and circumcoronene ($C_{54}H_{18}$) were selected because they span a large mass range and for their thermal stability at temperatures as high as 3000 K [22]. It was found that with an increase in PAH size, there was an increase in dimer stability (or equilibrium constant K_p). As temperature increases, K_p decreases which means that the PAH monomer is more stable than the dimer. The temperature for this crossover (K_p = 1 or Gibb's free energy of 0) was calculated to be 332 K for pyrene and 1387 K for circumcoronene. Both temperatures lie well below typical flame temperatures and this shows that PAHs as large as circumcoronene may not undergo a significant amount of dimerisation.

In addition MD simulations of the homomolecular clustering of the five PAHs were performed at five different temperatures (500, 750, 1000, 1250 and 1500 K) using the canonical NVT (moles-volume-temperature) ensemble with cubical periodic boundary conditions. The Nosé-Hoover thermostatting method [10, 15] was used to maintain a constant temperature with a time constant of 0.05 ps. Each simulation contained 1000 PAHs and was run for 1000 ps at a concentration of 2×10^{18} PAHs/cm^3 which corresponds to 4 ms and 1×10^{15} PAHs/cm^3, respectively, in actual flames. Inflated concentrations had to be used to account for the differing timescales between actual flames and that which is possible in MD simulations. To specify what constitutes a cluster and to control the stability of the cluster, two parameters have to be specified: a critical cut-off separation between two PAHs r_{crit} and a critical time length the two PAHs remain bound t_{crit}. The choice of r_{crit} = 12 Å and t_{crit} = 20 ps was somewhat arbitrary but these values were chosen so as to suppress the number of clusters detected.

Figure 7 shows the trajectories of each of the five systems at the lowest system temperature of 500 K. Five runs were carried out for each of the systems and averaged to show the average proportion of PAHs that are part of a cluster and the maximum number of PAHs in any one cluster. This figure clearly shows that pyrene dimerisation cannot play a significant role in soot particle formation even at low temperatures; at 1500 K only circumcoronene was found to dimerize (not shown). To conclude, for the physical binding of PAHs based on van der Waals interactions large PAH molecules of the order of 50 carbon atoms are required.

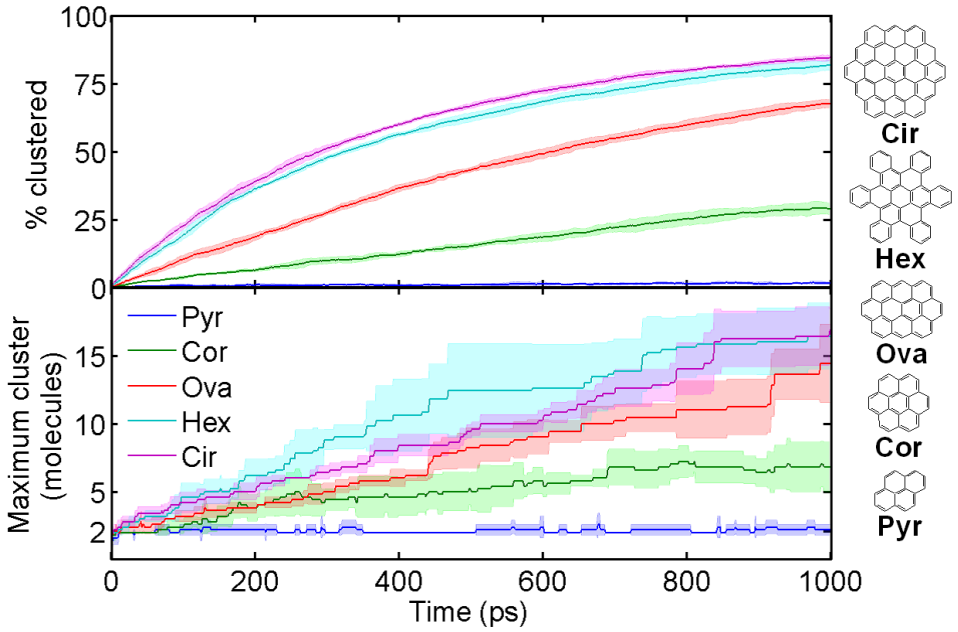

Figure 7: *Molecular dynamics results at 500 K for pyrene (Pyr), coronene (Cor), ovalene (Ova), hexabenzocoronene (Hex) and circumcoronene (Cir) where intermolecular interactions were modelled using the PAHAP potential as performed by Totton et al. [25]*

5.2 Combined PAH-PP/KMC-ARS Model[5]

The PAH-PP model, which is a population balance model, and the KMC-ARS model, which is a PAH surface growth model, are combined to study the coagulation of PAHs and their clusters in laminar premixed ethylene flames.

The following assumptions are made: (1) the rate of surface growth of a PAH in a stack is independent of the number of PAHs in the stack. This implies that the PAH surface growth processes are independent of the transformation processes that occur on a particle; (2) all reactive sites on a cluster or stack, regardless of position or orientation, are equally accessible to gas-phase species. Note that the term cluster refers to randomly orientated PAHs while stacks are PAHs aligned parallel to each other.

The rate of coagulation between two colliding PAHs a and b is calculated as:

$$R_{C_{a,b}} = C_E \times E_F \times \beta_{A,B} \times C_a \times C_b, \tag{15}$$

where C_E is the collision efficiency, $E_F = 2.2$ is the van der Waals enhancement factor [9], $\beta_{A,B}$ is the coagulation kernel, and C_a and C_b are the concentrations of PAHs a and b. An expression for $\beta_{A,B}$ in the free-molecular regime was found by Frenklach and Wang [5], while the concentrations of PAHs are easily obtained from the simulation.

In order to calculate the rate of coagulation C_E is required. A correlation for C_E was

[5] All material has been drawn from [18] unless otherwise indicated.

found through qualitative comparisons between computed and observed mass spectra. The laminar premixed ethylene flames studied by Happold [8] were chosen because of the availability of mass spectra. However, in these spectra, the concentrations of PAHs were measured in terms of varying intensities of ion signals for different PAH masses (monomers and dimers) which offered no direct comparison with computed number densities. Comparisons were made on the basis of three key features:

(1) Position of the maxima of PAH dimers;

(2) Position where there is a sharp decay in monomers;

(3) Spread of the dimer mass spectra on either side of the maxima: position where dimer spectra starts and ends.

C_{E} was found to depend on the diameter and mass of the smaller of the two colliding PAH clusters: D_{min} and M_{min} respectively. The following functional form was suggested:

$$C_{\mathrm{E}} = \frac{1}{1+\exp\left(-\left(A \times \frac{D_{\mathrm{min}}^3}{M_{\mathrm{min}}} + \left(\frac{M_{\mathrm{min}}}{B}\right)^6 - C\right)\right)}, \tag{16}$$

where A = 2 g/(mol.Å^3), B = 980 g/mol and C = 10 (dimensionless) are fitting parameters which give a good agreement between the computed and observed mass spectra on the basis of the above three features.

Figure 8 is a contour plot of C_{E} against D_{min} and M_{min}. The line for peri-condensed PAH monomers separates clusters made up of two or more PAHs, such as the $C_{38}H_{16}$ dimer shown, from the monomers below the line. It is observed that increasing D_{min} and M_{min} increases C_{E}. A reasonable amount of coagulation can be expected for $C_{\mathrm{E}} \geq 4$ % which corresponds to D_{min} = 360 amu and M_{min} = 10 Å. Pyrene has a mass of about 200 amu and a diameter of about 7 Å, which means that collisions involving pyrene is highly unlikely to be successful. Note that C_{E} does not account for changes in pressure and was fitted to high-temperature flames of about 1800 K.

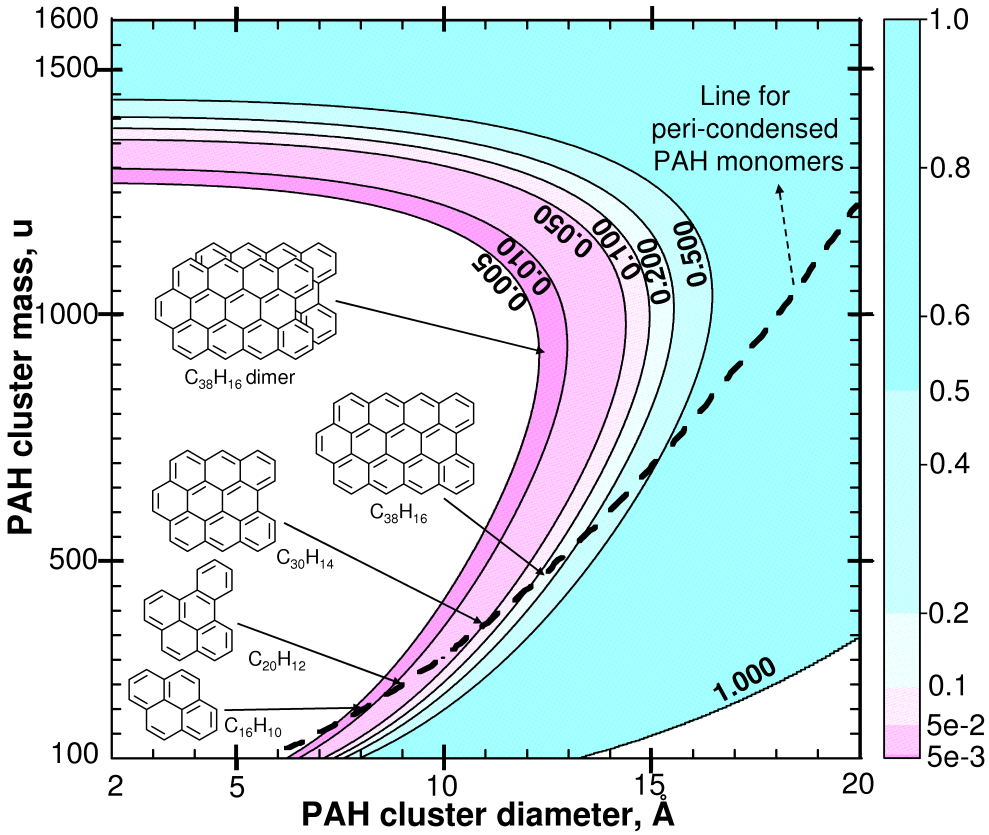

Figure 8: *Contour plot of collision efficiency used to calculate coagulation rates in the combined PAH-PP/KMC-ARS model (Raj et al. [18]; Copyright Elsevier)*

6 Conclusion

Several aspects of soot modelling have been discussed. The PAH-PP model combined with the KMC-ARS model describes soot particles in terms of its composition and shape. It also couples the particle to the surrounding gas-phase by tracking the gas-phase interactions of PAHs inside each primary particle. In addition two different potentials were used, which describe the forces between PAHs, to investigate the structure of nascent particles using basin hopping and MD. Both the combined PAH-PP/KMC-ARS model and MD were used to investigate the critical PAH size for successful dimerisation.

7 Final remarks

In this section, the similarities and differences between two approaches to soot modelling are discussed, namely the advanced multi-sectional method [4] and the PAH-PP/KMC-ARS model (Sects. 2 and 4; referred to as the stochastic model from hereon). In the sectional model particles are numerically treated as gas-phase species and by using lumped species, the numbers of carbon and hydrogen atoms are tracked. Also three different

morphologies are considered: large molecules, cluster of molecules (i.e. single particles) and agglomerates of particles. The stochastic model contains the most detailed particle description that is currently available, with thousands of internal coordinates tracked, including not just chemical composition but morphology. From this detailed description, TEM images and mass spectra have been computationally generated.

In the sectional model, the largest gas-phase species is determined by the chemical mechanism used. In this case it is pyrene which has 16 carbon atoms. All species with a larger molecular weight are conceptually treated as particles but numerically are treated as in the gas-phase. The mass range of these particles is defined by a range of sections and each section is assigned an average molecular weight and H/C ratio ranging from 0 to 1. The number of carbon atoms ranges from 24 in the first section to 2×10^{10} in the last section. In each section, the three different morphologies are considered. In the stochastic model each PAH is represented by the number of carbon and hydrogen atoms it contains, and the number and types of elementary sites on its edge. Primary particles are made up of PAH clusters and the connectivity between primary particles is stored using a binary tree structure. In both models, the orientation of the PAHs or PAH stacks which makes up a primary particle is not known.

Both models allow for the inception, coagulation, condensation, and surface growth and oxidation of particles but it is in the treatment of some of these processes where the models differ. The sectional model accounts for the inception process, i.e. the formation of the first particles or particle nuclei, both through the sticking of gas-phase PAHs and through the formation of large, polymer-like molecules that can coagulate forming the first particle. The coagulation efficiency used is size-dependent, approaching unity as the size of colliding particles increases. The model is also a function of the temperature and the interaction potential between coagulation entities. It has been confirmed by comparison with experimental data obtained at flame temperatures. Finally two different coagulation efficiencies are used for the coalescence and agglomeration times, allowing both single particles, up to a certain size, and agglomerates of particles, for larger compounds, to be considered. In the stochastic model, inception is the successful sticking of any two PAHs as determined by the collision efficiency model. An empirical correlation is used with a dependence on the diameter and mass of the smaller of the two colliding PAH clusters. The parameters of the model were obtained by fitting to various features of experimental mass spectra. Characteristic coalescence and agglomeration times are calculated in a similar fashion.

In the sectional model condensation and surface growth events increase the total mass of the particles. It accounts for the dehydrogenation process which allows for the lowering of the hydrogen content in particles typical of gas-phase PAHs to very low values typical of large soot aggregates. The gas-phase chemistry and particle phase are fully coupled and the chemical evolution of PAHs and particles is tracked. The stochastic model accounts for the increase in sphericity between any two primary particles in addition to accounting for the increase in mass. The exact structure and growth of each individual PAH is known. Although the particle dynamics and the chemical evolution of PAHs are fully coupled, it is not coupled to the gas-phase. Gas-phase species profiles computed using the PREMIX code with a method-of-moments soot model are fed as an input to the model.

Both models are able to account for the depletion of particles through surface oxidation.

A novel aspect of the sectional model is the ability to take into account oxidation-induced fragmentation of soot aggregates and particles. The process is triggered after a critical fraction of carbon atoms is removed from the aggregate/ particle. The fragmentation process has yet to be added to the stochastic model.

Abbreviations

C Carbon

DFT Density functional theory

DSA Direct simulation algorithm

DSMC Direct simulation Monte-Carlo

H Hydrogen

KMC Kinetic Monte-Carlo

KMC-ARS Kinetic Monte-Carlo-aromatic site

LJ Lennard-Jones

MD Molecular dynamics

PAH Polycyclic aromatic hydrocarbon

PAH-PP Polycyclic aromatic hydrocarbon-primary particle

PAHAP Polycyclic aromatic hydrocarbon anisotropic potential

PES Potential energy surface

PSD Particle size distribution

SAPT Symmetry adapted perturbation theory

TEM Transmission electron microscope

TST Transition state theory

References

[1] J. Appel, H. Bockhorn, and M. Frenklach. Kinetic modeling of soot formation with detailed chemistry and physics: laminar premixed flames of C_2 hydrocarbons. *Combustion and Flame*, 121:122–136, 2000. doi:10.1016/S0010-2180(99)00135-2.

[2] M. Celnik, A. Raj, R. West, R. Patterson, and M. Kraft. Aromatic site description of soot particles. *Combustion and Flame*, 155:161–180, 2008. doi:10.1016/j.combustflame.2008.04.011.

[3] D. Chen, Z. Zainuddin, E. Yapp, J. Akroyd, S. Mosbach, and M. Kraft. A fully coupled simulation of PAH and soot growth with a population balance model. *Proceedings of the Combustion Institute*, 34:1827–1835, 2013. doi:10.1016/j.proci.2012.06.089.

[4] A. D'Anna and M. Sirignano. An advanced multi-sectional method for particulate matter modeling in flames. In F. Battin-Leclerc, J. M. Simmie, and E. Blurock, editors, *Cleaner Combustion*, Green Energy and Technology, pages 363–388. Springer: London, 2013. doi:10.1007/978-1-4471-5307-8_14.

[5] M. Frenklach and H. Wang. Detailed mechanism and modeling of soot particle formation. In H. Bockhorn, editor, *Soot formation in combustion–mechanisms and models*, Springer Series in Chemical Physics, pages 165–190. Berlin: Springer, 1994.

[6] M. Frenklach, C. A. Schuetz, and J. Ping. Migration mechanism of aromatic-edge growth. *Proceedings of the Combustion Institute*, 30:1389–1396, 2005. doi:10.1016/j.proci.2004.07.048.

[7] B. Gómez-Lor, C. Koper, R. H. Fokkens, E. J. Vlietstra, T. J. Cleij, L. W. Jenneskens, N. M. M. Nibbering, and A. M. Echavarren. Zipping up 'the crushed fullerene' $C_{60}H_{30}$: C_{60} by fifteen-fold, consecutive intramolecular H_2 losses. *Chemical Communications*, pages 370–371, 2002. doi:10.1039/b110587f.

[8] J. Happold. *Geschichtete polyzyklische aromatische kohlenwasserstoffe als bausteine der rußbildung*. PhD thesis, Universität Stuttgart, 2008.

[9] S. J. Harris and I. M. Kennedy. The coagulation of soot particles with van der Waals forces. *Combustion Science and Technology*, 59:443–454, 1988. doi:10.1080/00102208808947110.

[10] W. Hoover. Canonical dynamics: equilibrium phase-space distributions. *Physical Review A*, 31:1695–1697, 1985. doi:10.1103/PhysRevA.31.1695.

[11] R. J. Kee, J. F. Grcar, M. D. Smooke, J. A. Miller, and E. Meeks. PREMIX: a FORTRAN program for modeling steady laminar one-dimensional premixed flames, SANDIA Report SAND85-8240. Technical report, Sandia National Laboratories, 1985.

[12] Z. Li and H. A. Scheraga. Monte Carlo-minimization approach to the multiple-minima problem in protein folding. *Proceedings of the National Academy of Sciences of the United States of America*, 84:6611–5, 1987.

[13] S. Mosbach, M. S. Celnik, A. Raj, M. Kraft, H. R. Zhang, S. Kubo, and K.-O. Kim. Towards a detailed soot model for internal combustion engines. *Combustion and Flame*, 156:1156–1165, 2009. doi:10.1016/j.combustflame.2009.01.003.

[14] M. Mueller, G. Blanquart, and H. Pitsch. Modeling the oxidation-induced fragmentation of soot aggregates in laminar flames. *Proceedings of the Combustion Institute*, 33:667–674, 2011. doi:10.1016/j.proci.2010.06.036.

[15] S. Nosé. A molecular dynamics method for simulations in the canonical ensemble. *Molecular Physics*, 52:255–268, 1984. doi:10.1080/00268978400101201.

[16] A. Raj, M. Celnik, R. Shirley, M. Sander, R. Patterson, R. West, and M. Kraft. A statistical approach to develop a detailed soot growth model using PAH characteristics. *Combustion and Flame*, 156:896–913, 2009. doi:10.1016/j.combustflame.2009.01.005.

[17] A. Raj, P. L. Man, T. S. Totton, M. Sander, R. A. Shirley, and M. Kraft. New polycyclic aromatic hydrocarbon (PAH) surface processes to improve the model prediction of the composition of combustion-generated PAHs and soot. *Carbon*, 48: 319–332, 2010. doi:10.1016/j.carbon.2009.09.030.

[18] A. Raj, M. Sander, V. Janardhanan, and M. Kraft. A study on the coagulation of polycyclic aromatic hydrocarbon clusters to determine their collision efficiency. *Combustion and Flame*, 157:523–534, 2010. doi:10.1016/j.combustflame.2009.10.003.

[19] A. Raj, G. R. da Silva, and S. H. Chung. Reaction mechanism for the free-edge oxidation of soot by O2. *Combustion and Flame*, 159:3423–3436, 2012. doi:10.1016/j.combustflame.2012.06.004.

[20] M. Sander. *Mathematical modelling of nanoparticles from the gas-phase*. PhD thesis, University of Cambridge, 2011.

[21] M. Sander, R. I. Patterson, A. Braumann, A. Raj, and M. Kraft. Developing the PAH-PP soot particle model using process informatics and uncertainty propagation. *Proceedings of the Combustion Institute*, 33:675–683, 2011. doi:10.1016/j.proci.2010.06.156.

[22] S. E. Stein and A. Fahr. High-temperature stabilities of hydrocarbons. *The Journal of Physical Chemistry*, 89:3714–3725, 1985. doi:10.1021/j100263a027.

[23] K. T. Tang and J. P. Toennies. An improved simple model for the van der Waals potential based on universal damping functions for the dispersion coefficients. *The Journal of Chemical Physics*, 80:3726, 1984. doi:10.1063/1.447150.

[24] T. S. Totton, D. Chakrabarti, A. J. Misquitta, M. Sander, D. J. Wales, and M. Kraft. Modelling the internal structure of nascent soot particles. *Combustion and Flame*, 157:909–914, 2010. doi:10.1016/j.combustflame.2009.11.013.

[25] T. S. Totton, A. J. Misquitta, and M. Kraft. A quantitative study of the clustering of polycyclic aromatic hydrocarbons at high temperatures. *Physical chemistry chemical physics : PCCP*, 14:4081–94, 2012. doi:10.1039/c2cp23008a.

[26] B. W. van de Waal. Calculated ground-state structures of 13-molecule clusters of carbon dioxide, methane, benzene, cyclohexane, and naphthalene. *The Journal of Chemical Physics*, 79:3948, 1983. doi:10.1063/1.446263.

[27] D. J. Wales and J. P. K. Doye. Global optimization by basin-hopping and the lowest energy structures of Lennard-Jones clusters containing up to 110 atoms. *The Journal of Physical Chemistry A*, 101:5111–5116, 1997. doi:10.1021/jp970984n.

[28] H. Wang. Formation of nascent soot and other condensed-phase materials in flames. *Proceedings of the Combustion Institute*, 33:41–67, 2011. doi:10.1016/j.proci.2010.09.009.

[29] B. Zhao, Z. Yang, Z. Li, M. V. Johnston, and H. Wang. Particle size distribution function of incipient soot in laminar premixed ethylene flames: effect of flame temperature. *Proceedings of the Combustion Institute*, 30:1441–1448, 2005. doi:10.1016/j.proci.2004.08.104.